Contrib Mineral Petrol (2015) 169:2
DOI 10.1007/s00410-014-1097-0

ORIGINAL PAPER

Phase relations and formation of chromium-rich phases in the system $Mg_4Si_4O_{12}$–$Mg_3Cr_2Si_3O_{12}$ at 10–24 GPa and 1,600 °C

E. A. Sirotkina · A. V. Bobrov · L. Bindi · T. Irifune

Received: 19 August 2014 / Accepted: 12 December 2014

Abstract Phase relations in the system $Mg_4Si_4O_{12}$–$Mg_3Cr_2Si_3O_{12}$ were studied at 10–24 GPa and 1,600 °C using a high-pressure Kawai-type multi-anvil apparatus. We investigated the full range of starting compositions for the knorringite–majorite system to derive a *P–X* phase diagram and synthesize garnets of a wide compositional range. Samples synthesized in the pressure range 10–14 GPa contain knorringite–majorite garnet and Cr-bearing pyroxene. With increasing Cr content in the starting materials, an association of knorringite–majorite garnet and eskolaite is formed. Garnets contain a significant portion of majorite (>10 mol%) even for a pure $Mg_3Cr_2Si_3O_{12}$ starting composition. Knorringite–majorite garnets were obtained in the pressure range from 10 to 20 GPa. With increasing pressure, the phase assemblages include Cr-bearing $MgSiO_3$ akimotoite and $MgSiO_3$ bridgmanite, as well as $MgCr_2O_4$ with calcium titanate structure, and stishovite. Single-crystal X-ray diffraction shows that the incorporation of Cr into the structure of garnet, as well as $MgSiO_3$ akimotoite, and bridgmanite results in an increase in their unit cell parameters. Results of the experimental high-pressure investigation of the pseudo-binary system $Mg_4Si_4O_{12}$–$Mg_3Cr_2Si_3O_{12}$ (SiO_2–MgO–Cr_2O_3) may be applied to the origin of high chromium phases (mostly garnet) found as inclusions in peridotitic diamonds and formed in bulk rock compositions with high Cr/Al ratios in relation to the primitive mantle.

Keywords Knorringite · Majorite · Bridgmanite · Akimotoite · Mantle · High *P–T* experiments · Phase relations

Abbreviations

Ak	Akimotoite ($MgSiO_3$ with ilmenite-type structure)
Al-Ak	Aluminum-rich akimotoite
Al-Brd	Aluminum-rich bridgmanite
Brd	Bridgmanite ($MgSiO_3$ with perovskite-type structure)
Cr-Ak	Chromium-rich akimotoite
Cr-Brd	Chromium-rich bridgmanite
Ct	$MgCr_2O_4$ with calcium titanate structure
Esk	Eskolaite (Cr_2O_3)
Grt	Garnet
Knr	Knorringite ($Mg_3Cr_2Si_3O_{12}$)
Maj	Majorite ($Mg_4Si_4O_{12}$)
Prp	Pyrope ($Mg_3Al_2Si_3O_{12}$)
Px	Pyroxene
Sti	Stishovite

Communicated by Timothy L. Grove.

E. A. Sirotkina (✉) · A. V. Bobrov
Department of Petrology, Geological Faculty, Moscow State University, Leninskie Gory, 119991 Moscow, Russia
e-mail: katty.ea@mail.ru

L. Bindi
Dipartimento di Scienze della Terra, Università di Firenze, Via La Pira 4, 50121 Florence, Italy

L. Bindi
CNR – Istituto di Geoscienze e Georisorse, Sezione di Firenze, Via La Pira 4, 50121 Florence, Italy

T. Irifune
Geodynamics Research Center, Ehime University, Matsuyama 790-8577, Japan

T. Irifune
Earth-Life Science Institute, Tokyo Institute of Technology, Tokyo 152-8550, Japan

Published online: 10 January 2015

Introduction

The problem of the composition and structure of deep Earth have been debated over the past decades. It is generally considered that a relatively small group of elements (Si, Mg, Fe, Al, Ca, and O) is predominant in Earth's interior. They mostly form the main phases of the upper mantle (olivine, ortho- and clinopyroxene, garnet), transition zone (wadsleyite, ringwoodite, and majoritic garnet), and the lower mantle (bridgmanite, magnesiowüstite, and $CaSiO_3$ perovskite), which are responsible for the global seismic boundaries (e.g. Pushcharovsky and Pushcharovsky 2012). However, models of the chemical and phase composition of deep Earth also should account for the high-pressure behavior of minor elements and, in particular, potential phases accumulating these elements at mantle depths. The solubility of minor elements in high-pressure phases is poorly studied, although even small concentrations of these elements may significantly influence the physical properties of mantle phases. Minor elements sometimes control the physicochemical parameters of the main phase equilibria, as well as the crystal-chemical peculiarities of mantle phases.

One of such elements is chromium, which, in spite of the low bulk concentrations in the Earth's mantle (0.42 wt% Cr_2O_3; Ringwood 1966), may be significantly accumulated in mantle minerals such as garnet and bridgmanite: The concentration of Cr_2O_3 in natural garnets reaches 20 wt% (Stachel and Harris 1997), whereas bridgmanite included in diamonds formed in the lower mantle contains up to 1.2 wt% Cr_2O_3 (Harte et al. 1999).

Knorringite, $Mg_3Cr_2Si_3O_{12}$, is usually found either in rocks from the deep lithospheric mantle or as inclusions in diamonds and constituents of ultramafic mantle xenoliths (Sobolev 1977; Meyer 1987; Taylor and Anand 2004). As it was originally shown by Malinovskii et al. (1975), incorporation of the knorringite component in garnet occurs from 3 GPa and the concentration of chromium achieves significant values (5–10 wt% Cr_2O_3 and more) in the pressure range of origin of most natural diamonds (i.e., 4–7 GPa). These features imply a correlation between the composition of peridotitic garnet and the conditions of diamond formation, so that Cr-rich pyropic garnet (as well as Cr-rich spinel) is usually the most important diamond indicator mineral used in the diamond exploration (Grüter et al. 2006).

Although knorringite is an important end member of garnet in the deep lithospheric mantle, the stability and high-pressure phase relations of knorringite are still controversial. Its stability field has been investigated in several studies (Ringwood 1977; Irifune et al. 1982; Turkin et al. 1983; Klemme 2004; Taran et al. 2004; Zou and Irifune 2012). Ringwood (1977) synthesized knorringitic garnet in a quite wide pressure range (6–8 GPa) at temperatures of 1,400–1,500 °C. Irifune et al. (1982) demonstrated the stability of knorringite at pressures >11.5 GPa at 1,200 °C and at >11.8 GPa at 1,400 °C. By contrast, Turkin et al. (1983) reported on the appearance of knorringite at significantly lower pressures of 8.0–9.5 GPa at 1,200–1,800 °C with a negative slope of the phase boundary. Klemme (2004) synthesized knorringite coexisting with eskolaite (Cr_2O_3) at 16 GPa and 1,600 °C. Taran et al. (2004) reported on the synthesis of knorringite at 9–16 GPa and 1,300–1,600 °C.

The structure of knorringite was refined by X-ray single crystal (Bykova et al. 2014) and powder diffraction studies (Juhin et al. 2010). Wijbrans et al. (2014) reported thermodynamic and magnetic properties of knorringite based on low-temperature calorimetric data and magnetic susceptibility measurements.

Recently, it was demonstrated that knorringitic garnet synthesized in high-pressure experiments always contained an admixture of majorite ($Mg_4Si_4O_{12}$), which resulted in the appearance of eskolaite in run products (Juhin et al. 2010; Zou and Irifune 2012), even when knorringite garnet with the composition very close to $Mg_3Cr_2Si_3O_{12}$ was synthesized (Klemme (2004). This is consistent with the composition of some Cr-bearing majoritic garnets included in natural diamonds of the peridotitic assemblage (Fig. 1).

The concentration of aluminum and chromium in garnets decreases with pressure (Akaogi and Akimoto 1977; Irifune 1987), whereas the content of silicon in the octahedral site, as well as the concentration of divalent cations (Ca, Mg, Fe) and sodium increases (Ono and Yasuda 1996), which results in the formation of garnet with a silicon content of >3 p.f.u (Fig. 1a). This is controlled by the beginning of dissolution of pyroxene (mainly $(Mg,Fe)SiO_3$) components in garnet already from 7.5 GPa (Akaogi and Akimoto 1979). The solubility of pyroxene in garnet increases with pressure, reaching significant values at 10–15 GPa, which corresponds to the lowermost upper mantle and transition zone. In a Cr–Si diagram (Fig. 1b), peridotite garnet inclusions in diamond plot on two major compositional trends: pyrope–majorite and pyrope–knorringite. However, some garnets with relatively low pyrope content (e.g., S1–30) plot away from these trends, showing the presence of knorringite-rich majoritic garnet. One high chromium majoritic garnet with ~20 wt% CaO (Yum-27) belongs to the wehrlitic paragenesis and contains a high concentration of the uvarovite component rather than knorringite component.

Thus, knorringite and majorite are the high-pressure components of natural pyrope garnets of the peridotitic assemblage. The pyrope–majorite (Akaogi and Akimoto 1977) and pyrope–knorringite (Malinovskii and Doroshev 1974; Ringwood 1977; Klemme 2004; Turkin and Sobolev 2009) joins have been deeply studied experimentally. High-pressure and high-temperature phase relations for $Mg_3Cr_2Si_3O_{12}$ have been investigated at pressures from 8 to 16

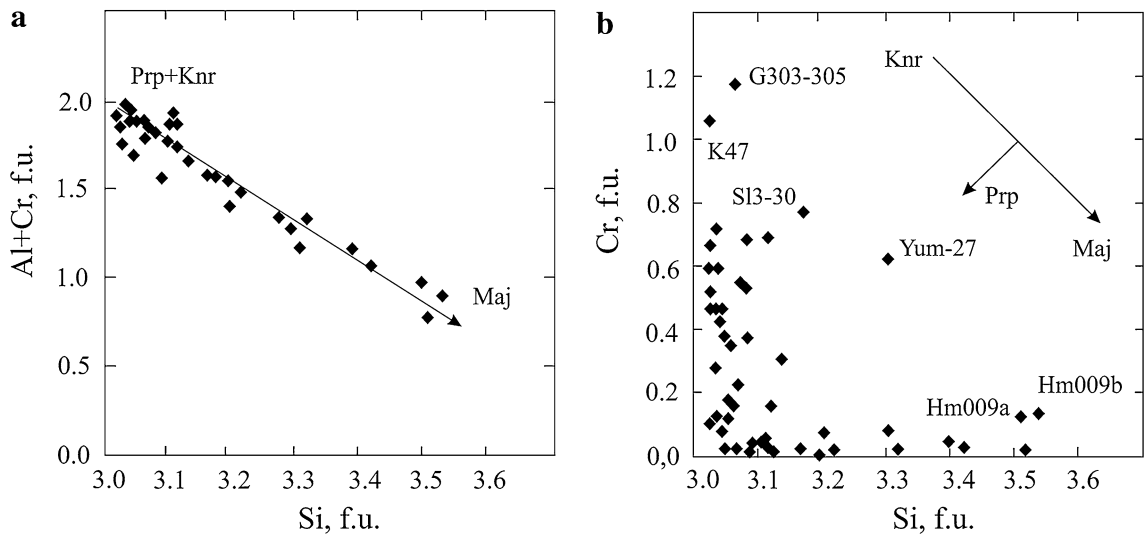

Fig. 1 Compositional variations in chromium-bearing majoritic garnets from inclusions in natural diamonds (Stachel 2001; Taylor and Anand 2004). *Solid lines* with *arrows* indicate pyrope (+knorringite)–majorite (**a**) and knorringite–majorite (**b**) series. The labeled garnets are significantly depleted in pyrope, and their composition is the closest to the majorite–knorringite trend: G303-305 (Stachel and Harris 1997), K-47 (Nixon and Hornung 1968), S1-30 (Pokhilenko et al. 2004), Yum-27 (garnet of wehrlitic paragenesis; Sobolev et al. 2004), Hm009a and Hm009b (McKenna et al. 2004)

GPa and temperatures of 1,200–1,800 °C (Zou and Irifune 2012). Although both knorringite and majorite components are important for barometry of mantle mineral associations, the high-pressure phase relations in the Maj–Knr system have not been studied yet. Data on the high-pressure knorringite stability, as well as on post-garnet Cr-bearing phases, are also absent.

The current study is an extension of work of Zou and Irifune (2012) to higher pressures. Our experiments aimed to the study of phase relations, achieve synthesis of Cr-bearing phases (majoritic garnet, akimotoite, bridgmanite, and $MgCr_2O_4$ with a calcium titanate structure), and their solid solutions in the $Mg_4Si_4O_{12}$–$Mg_3Cr_2Si_3O_{12}$ system at 10–24 GPa and 1,600 °C, and to the study of the conditions of formation, structural peculiarities, and compositional changes of Cr-rich phases with pressure using a Kawai-type multi-anvil apparatus.

Experimental and analytical procedures

Powdered mixtures of chemically pure oxides (MgO, Cr_2O_3, and SiO_2) taken in stoichiometric proportions, homogenized at room temperature using ethanol, and then dried in the stove at 100 °C were used as starting materials. The use of fine-grained (<1 μm) oxides helps to enhance chemical reactions in H*P*–H*T* runs, as demonstrated by Zou and Irifune (2012). Nine compositions falling between the majorite $Mg_4Si_4O_{12}$ and knorringite $Mg_3Cr_2Si_3O_{12}$ end members were prepared.

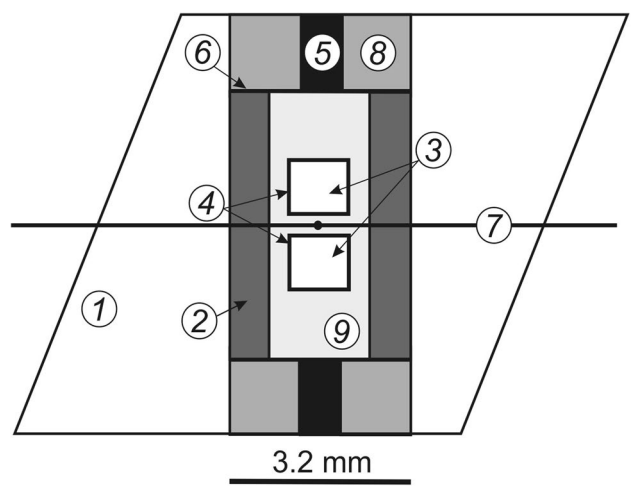

Fig. 2 Sample assembly of the Kawai-type apparatus used in this study: (1) semi-sintered 8-mm edged (Mg,Co)O octahedron; (2) $LaCrO_3$ tubular heater; (3) starting material (sample); (4) platinum capsule; (5) Mo electrodes; (6) Mo discs; (7) $W_{97}Re_3$–$W_{75}Re_{25}$ thermocouple; (8) ZrO_2 plugs; and (9) MgO cylinders, sleeves and MgO powder

The experiments were performed at pressures of 10–24 GPa and at a fixed temperature of 1,600 °C using a 2,000-t Kawai-type multi-anvil high-pressure apparatus at the Geodynamics Research Center, Ehime University (Matsuyama, Japan). The cell assembly used in the present experiments is shown in Fig. 2. Tungsten carbide cubic anvils with 4.0- and 2.5-mm truncation edge length were applied as the second-stage anvils of the high-pressure apparatus. The

pressure medium was a semi-sintered (Mg,Co)O octahedron of 10.0 and 8.0 mm in edge length. A tubular $LaCrO_3$ heater was inserted into the pressure medium. A starting mixture (sample) was loaded into a capsule of 1.1 mm in height and 1.2 mm in diameter made of a platinum foil. The capsule was insulated from the heater by a MgO sleeve.

The temperature was measured using a $W_{97}Re_3$–$W_{75}Re_{25}$ thermocouple with a hot junction positioned in the central part of the heater. The temperature measurement accuracy was ±10 °C. Pressure values at room temperature were calibrated against the load (oil pressure) of the press based on the pressure fixed points: Bi I–II transition at 2.55 GPa, Bi III–V transition at 7.7 GPa, and semiconductor–metal transitions of ZnS at 15.5 GPa and GaAs at 18.3 GPa (Irifune et al. 2004; Zou and Irifune 2012). The effect of temperature on pressure was further corrected using the α–β and β–γ phase transitions of Mg_2SiO_4 (Katsura and Ito 1989; Yamada et al. 2004). As a result, run pressure was controlled to ±0.5 GPa (Irifune et al. 1991). The experiments started with pressurization at ambient temperature to 10–24 GPa. Subsequently, the charge was heated to 1,600 °C. Duration of each run was 3–5 h. After the experiments, the samples were quenched by switching off the power supply, subsequently depressurized, and recovered at ambient conditions. As there was some temperature gradient within the sample, only the high-temperature portions near the thermocouple junction were examined in the following analyses.

Each run sample was divided into several pieces for microprobe analysis and XRD measurements. To analyze phase compositions, the samples were embedded into epoxy and polished. Compositions of synthesized phases were studied at the Geological Faculty, Moscow State University, by using a Jeol JSM-6480LV electron microscope equipped with an energy-dispersive X-ray detector INCA Energy. The following standards were used: synthetic SiO_2, MgO, and Cr_2O_3 for Si, Mg, and Cr, respectively. Phase compositions in each run were determined from the average of 2–6 analyses performed at 15 and 20 kV accelerating voltage, 15 and 10 nA beam current. The main criterion for considering the pyroxene or garnet analyses acceptable was the sum of cations for six oxygens being between 3.98 and 4.02. The samples were homogeneous, without significant differences in textures and mineral composition and without zoning of individual grains, thus confirming that the chemical equilibrium was achieved in the runs. We applied the SkyScan software (CT-An) for precise determination of the bulk concentration of garnet in the sample by using BSE images.

Small crystals of chromium-rich phases, including majorite–knorringite garnet, Cr-bearing $MgSiO_3$ akimotoite and bridgmanite, and $MgCr_2O_4$ calcium titanate, handpicked under a reflected light microscope from the experimental products were preliminarily examined with a Bruker–Enraf MACH3 single-crystal diffractometer using graphite-monochromatized MoKα radiation. The data collections were then done with an Oxford Diffraction Xcalibur 3 diffractometer (X-ray MoKα radiation, $\lambda = 0.71073$ Å) fitted with a Sapphire 2 CCD detector. Intensity integration and standard Lorentz-polarization corrections were done with the CrysAlis RED (Oxford Diffraction 2006) software package. The program ABSPACK of the CrysAlis RED package (Oxford Diffraction 2006) was used for the absorption correction.

Experimental results and discussion

P–X diagram for the system $Mg_4Si_4O_{12}$–$Mg_3Cr_2Si_3O_{12}$ at 1,600 °C and textural relationships in the run products

At 10–24 GPa and 1,600 °C, we studied the full range of the starting materials in the $Mg_4Si_4O_{12}$ (Maj)–$Mg_3Cr_2Si_3O_{12}$ (Knr) system in increments of 10–20 mol% Knr and 1–2 GPa, which allowed us to synthesize chromium-bearing phases with a wide compositional range. The main phases obtained in experiments were pyroxene, garnet of the Maj–Knr composition, Cr-bearing $MgSiO_3$ akimotoite and $MgSiO_3$ bridgmanite, eskolaite, $MgCr_2O_4$ with the calcium titanate-type structure, and stishovite. Run conditions and phase compositions of the samples are reported in Table 1.

Phase relations in the system $Mg_4Si_4O_{12}$–$Mg_3Cr_2Si_3O_{12}$ can be described in terms of the three-component system SiO_2–MgO–Cr_2O_3 (Fig. 3). The pseudo-binary $Mg_4Si_4O_{12}$–$Mg_3Cr_2Si_3O_{12}$ system is a small fragment of the *P–X* $MgSiO_3$–Cr_2O_3 section (Fig. 4) of the SiO_2–MgO–Cr_2O_3 diagram, which was studied by Zou and Irifune (2012) up to 16 GPa.

Garnet forms the majorite–knorringite solid solution series that is stable above ~8 GPa; at lower pressure, an association of pyroxene and eskolaite (En + Esk) is stable (Zou and Irifune 2012). Pyroxene with a small chromium admixture is associated with chromium-bearing majoritic garnet at pressures of 10–14 GPa and low chromium concentration in the starting material. The texture of the samples is formed by relatively large isometric garnet crystals and often large elongated pyroxene crystals with clear cleavage (Fig. 5a). The length of prismatic pyroxene grains reaches 120 μm. The portion of garnet in the sample increases with increasing chromium content in the starting composition: The content of garnet is ≤12 vol% in run 2,520–5 (5 mol% Knr in the starting composition), whereas the content of garnet in run 2,423–15 (15 mol% Knr in the starting composition) reaches 40 vol%.

Table 1 Run conditions and products of experiments in the join $MgSiO_3$–$Mg_3Cr_2Si_3O_{12}$

P (GPa)	Run number	N_{Knr}^{system}	Time (h)	Run products
10	2,526–100	100	5	Grt + Esk
	2,535–100	100	5	Grt + Esk
12	2,521–100	100	5	Grt + Esk
	2,404–100	100	4	Grt + Esk
	2,404–50	50	4	Grt + Px[a]
14	2,533–100	100	5	Grt + Esk
	2,403–100	100	4	Grt + Esk
	2,403–50	50	4	Grt
	2,423–15	15	4	Grt + Px
	2,520–5	5	5	Grt + Px
15	2,425–5	5	5	Grt
16	2,401–100	100	5	Grt + Esk
	2,397–100	100	4	Grt + Esk
	2,399–90	90	4	Grt + Esk
	2,397–70	70	4	Grt
	2,398–50	50	4	Grt
	2,418–15	15	5	Grt
	2,399–10	10	4	Grt
17	2,408–100	100	5	Grt + Esk
18	2,415–100	100	5	Grt + Ct + Sti
	2,438–60	60	5	Grt
	2,410–30	30	5	Grt + Ak
	2,415–10	10	5	Grt[a] + Ak
19	2,530–100	100	5	Grt + Ct[a] + Sti
	2,531–30	30	5	Grt + Ak
	2,531–15	15	5	Grt + Ak
	2,530–5	5	5	Ak
20	2,402–100	100	3	Grt + Ct + Sti
	2,407–90	90	4	Grt + Ct + Sti
	2,406–70	70	4	Grt + Ct[a] + Sti
	2,402–50	50	3	Grt + Brd + Ct + Sti
	2,407–30	30	4	Grt + Brd
	2,434–15	15	5	Brd
21	2,528–100	100	5	Brd + Ct + Sti
	2,528–30	30	5	Brd + Ct[a] + Sti
	2,529–10	10	5	Brd
23	2,413–70	70	4	Brd + Ct + Sti
24	2,424–50	50	4	Brd + Ct[a] + Sti
	2,424–10	10	4	Brd

[a] Because of the small grain sizes, compositions of the phases were not analyzed

Further increase in pressure and $Mg_3Cr_2Si_3O_{12}$ concentration in the starting materials results in the formation of a single-phase field of majorite–knorringite garnet (Fig. 4). This mineral forms large euhedral crystals with a size up to 150 μm. Increase in the concentration of the knorringite end member in the starting material results in appearance of an association of Cr-rich majoritic garnet and eskolaite, according to the following reaction:

$$Mg_3Cr_2Si_3O_{12}(Knr) = 3MgSiO_3(Maj) + Cr_2O_3(Esk) \quad (1)$$

Eskolaite plots outside the Knr–Maj section (line a) on the SiO_2–MgO–Cr_2O_3 diagram (Fig. 3), which is typical of a pseudo-binary system.

The texture of the experimental sample as shown in Fig. 5b is formed by relatively large garnet crystals with a size of >150 μm and small uniformly distributed eskolaite grains, often interstitial. Eskolaite is often observed as inclusions in garnet crystals. The size of the eskolaite grains is 10 μm. With increasing pressure, the field of Grt + Esk expands to lower Cr concentrations in the system due to decreasing Cr solubility in garnet. Thus, we assume that each pressure value is characterized by the defined maximum solubility of chromium in garnet. The modal proportion of eskolaite in this association increases with increasing chromium concentration in the starting material.

For Cr-poor bulk compositions (0–10 mol% Knr in the starting composition), a single-phase field of $MgSiO_3$ akimotoite opens up at pressures ≥~18 GPa (Fig. 4). This mineral forms massive aggregates (Fig. 5c) with a size of individual grains up to 100 μm. The presence of garnet in association with akimotoite is registered for the starting compositions with moderate chromium concentration (10–50 mol% Knr). Akimotoite associated with garnet is represented by large subhedral crystals with a size of <50 μm (Fig. 5d). With increasing pressure (up to 19 GPa), the proportion of garnet in the experimental sample decreases.

A paragenesis of garnet and Cr-bearing $MgSiO_3$ bridgmanite appears at 20 GPa (Fig. 4). The sample texture is formed by relatively large euhedral garnet crystals and smaller, subhedral bridgmanite grains with small fractures.

In the Cr-rich part of the system at ~17 GPa, an association of garnet and eskolaite is replaced by the paragenesis of garnet, stishovite, and the $MgCr_2O_4$ with a calcium titanate-type structure (Ct). The first appearance of Ct + Esk (line b in Fig. 3) is controlled by the reaction:

$$MgSiO_3(Maj) + Cr_2O_3(Esk) = MgCr_2O_4(Ct) + SiO_2(Sti). \quad (2)$$

The portion of garnet in experimental samples gradually decreases with increasing pressure, so that only rare garnet grains (<5 vol%) are registered at 20 GPa. Complete disappearance of garnet at a pressure of >20 GPa (Fig. 4) is controlled by the decomposition of knorringite through the reaction (compositional triangle c in Fig. 3):

$$Mg_3Cr_2Si_3O_{12}(Knr) = 2MgSiO_3(Brd) + MgCr_2O_4(Ct) + SiO_2(Sti). \quad (3)$$

Ct forms relatively large grains with a size up to 50 μm. Characteristically, stishovite appears in association with chromium-rich garnet or chromium-bearing bridgmanite

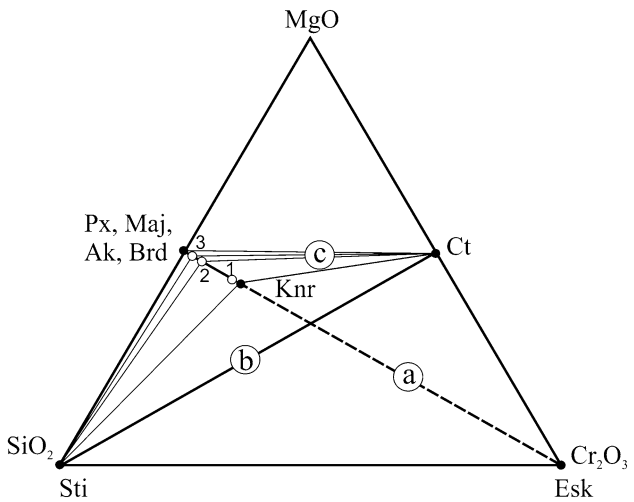

Fig. 3 Relative position of phases and the studied $Mg_4Si_4O_{12}$–$Mg_3Cr_2Si_3O_{12}$ system within the triangle SiO_2–MgO–Cr_2O_3. Numbers (1–3) indicate the maximum Cr_2O_3 concentrations in garnet (1), $MgSiO_3$ bridgmanite (2), and $MgSiO_3$ akimotoite (3) registered in the runs. *Letters in circles* (a–c) correspond to the sequence of chemical reactions with increasing pressure

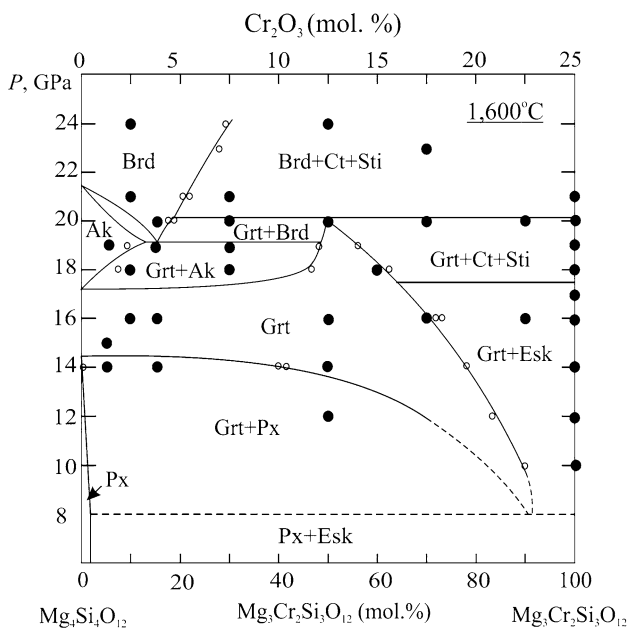

Fig. 4 *P–X* subsection $Mg_4Si_4O_{12}$–$Mg_3Cr_2Si_3O_{12}$ of the SiO_2–MgO–Cr_2O_3 phase diagram (Fig. 3). *Small open circles* denote the composition ("Knr", mol%) of the phases

and the $MgCr_2O_4$ phase. Stishovite forms small anhedral grains with a size up to 10 µm. The transition from garnet-bearing associations (Grt + Brd and Grt + Ct + Sti) to the paragenesis of $MgSiO_3$ bridgmanite (Brd + Ct + Sti) (Fig. 5e) is observed in a wide compositional range (10–100 mol% Knr) of starting materials at ~20 GPa (Fig. 4).

Fig. 5 BSE images of textural relationships in some run products in the system $Mg_4Si_4O_{12}$–$Mg_3Cr_2Si_3O_{12}$ at 10–24 GPa and 1,600 °C. **a** Aggregate of majorite–knorringite garnet and prismatic pyroxene grains. **b** Association of majorite–knorringite garnet and eskolaite occurring as inclusions in garnet and filling interstitials. **c** massive aggregate of subhedral $MgSiO_3$ akimotoite grains. **d** Segregation of small $MgSiO_3$ akimotoite grains in majorite–knorringite garnet. **e** Aggregate of $MgSiO_3$ bridgmanite, $MgCr_2O_4$ with a calcium titanate-type structure, and stishovite. **f** Massive aggregate of bridgmanite grains with a dense system of fractures

The single-phase field of $MgSiO_3$ bridgmanite is typical of low chromium starting compositions at pressures of >20 GPa. Bridgmanite forms massive fractured aggregates with a grain size of up to 50 µm (Fig. 5f).

Compositions of the phases

Most phases synthesized in the system $Mg_4Si_4O_{12}$–$Mg_3Cr_2Si_3O_{12}$ at 10–24 GPa and 1,600 °C show wide compositional variations. Compositions of the phases produced in our experiments are reported in Table 2. *Pyroxene* in run products has enstatitic composition with a small chromium admixture (<0.6 wt% Cr_2O_3, 0.008 pfu).

Garnets in all experimental samples are characterized by a silicon surplus over 3.0 pfu Si, indicating incorporation of the majorite end member. Garnet associated with pyroxene has quite high concentrations of chromium (up to 24 wt% Cr_2O_3, 1.359 Cr pfu). The concentration of chromium decreases with increasing pressure (14 wt% Cr_2O_3, 0.801 Cr pfu at 14 GPa), which is explained by an increase in the total content of garnet and a decrease of the pyroxene portion in the samples. The maximum knorringite component in garnets synthesized in the single-phase garnet area of the system (Fig. 4) decreases with pressure.

Garnet associated with eskolaite becomes depleted in chromium with increasing pressure, whereas the concentration of sixfold coordinated silicon (majorite component) increases (Fig. 6a). There is also a negative correlation between Mg and Cr in garnet (Fig. 6b) showing the coupled substitution of Cr^{3+} by $Mg^{2+}+Si^{4+}$ in knorringite garnet.

Garnet associated with akimotoite at a pressure of >17 GPa becomes enriched in Cr (17–18 wt% Cr_2O_3, ~1.005 Cr pfu), due to the inability of akimotoite to incorporate greater amounts of chromium. In this case, the composition of garnet does not depend on the starting composition and is controlled by pressure. The proportion of garnet decreases, and the concentration of chromium in Grt increases with pressure. At $P \geq 19$ GPa, garnet is accompanied by bridgmanite that does not have much influence on the composition of garnet. The concentration of Cr_2O_3 in garnet associated with bridgmanite reaches 18 wt% (1.030 Cr pfu).

The study of starting compositions corresponding to pure $Mg_3Cr_2Si_3O_{12}$ is very important with respect to

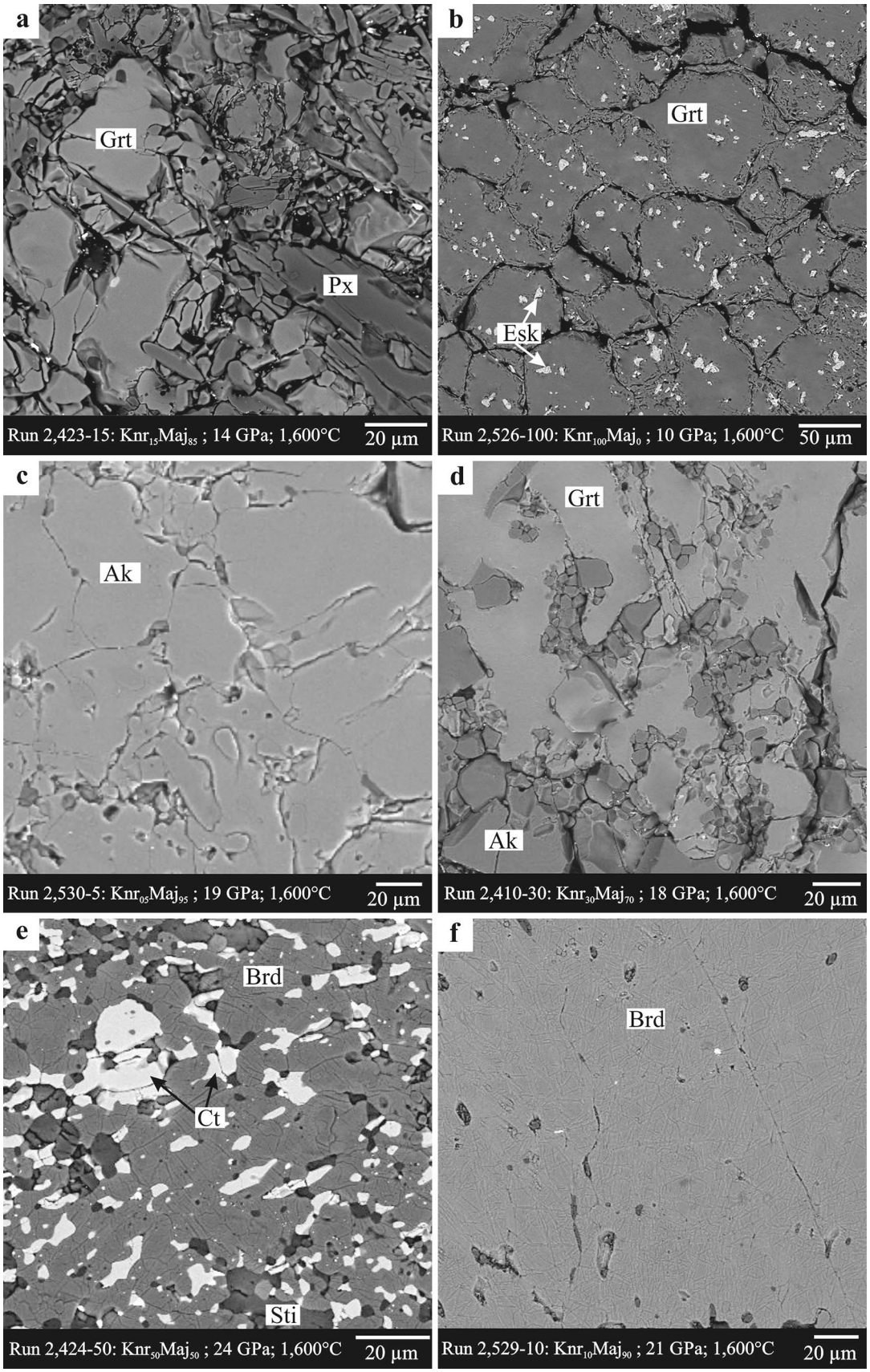
a
Grt
Px
Run 2,423-15: $Knr_{15}Maj_{85}$; 14 GPa; 1,600°C
20 µm
b
Grt
Esk
Run 2,526-100: $Knr_{100}Maj_{0}$; 10 GPa; 1,600°C
50 µm
c
Ak
Run 2,530-5: $Knr_{05}Maj_{95}$; 19 GPa; 1,600°C
20 µm
d
Grt
Ak
Run 2,410-30: $Knr_{30}Maj_{70}$; 18 GPa; 1,600°C
20 µm
e
Brd
Ct
Sti
Run 2,424-50: $Knr_{50}Maj_{50}$; 24 GPa; 1,600°C
20 µm
f
Brd
Run 2,529-10: $Knr_{10}Maj_{90}$; 21 GPa; 1,600°C
20 µm

Table 2 Mean composition of phases produced in the join $MgSiO_3$–$Mg_3Cr_2Si_3O_{12}$ at 10–24 GPa and 1,600 °C

P, GPa	10		12			14			
Run no.	2,526–100		2,521–100		2,404–50	2,533–100		2,423–15	
Phase	Grt[a]	Esk	Grt	Esk	Grt	Grt	Esk	Grt	Px
Number of points	4	5	5	4	4	5	3	6	3
MgO	28.16 (0.54)	0.30 (0.11)	29.01 (0.05)	1.55 (0.40)	31.01 (0.39)	32.35 (0.31)	1.51 (0.32)	34.62 (0.25)	39.73 (0.20)
SiO_2	41.24 (0.43)	0.47 (0.2)	43.21 (0.12)	1.54 (0.28)	45.81 (0.48)	47.93 (0.30)	1.69 (0.31)	50.59 (0.37)	58.71 (0.21)
Cr_2O_3	30.78 (0.20)	98.45 (0.79)	28.70 (0.09)	94.99 (0.35)	23.79 (0.36)	19.99 (0.25)	96.26 (0.45)	14.35 (0.08)	0.6 (0.08)
Total	100.18	99.22	100.91	98.08	100.61	100.27	99.46	99.56	99.04
Formula units per given O									
O	12	3	12	3	12	12	3	12	3
Mg	3.128	0.011	3.169	0.059	3.339	3.240	0.056	3.644	1.001
Si	3.075	0.012	3.169	0.039	3.311	3.212	0.042	3.576	0.993
Cr	1.814	1.976	1.663	1.909	1.359	1.557	1.905	0.801	0.008
Total	8.018	2.000	8.000	2.006	8.009	8.009	2.004	8.021	2.003

P, GPa	14			15	16				
Run no.	2,403–50	2,520–5		2,425–5	2,401–100		2,399–90		2,397–70
Phase	Grt	Grt	Px	Grt[a]	Grt	Esk	Grt	Esk	Grt
Number of points	3	6	4	4	7	3	6	1	5
MgO	33.52 (0.28)	34.36 (0.31)	39.86 (0.37)	39.62 (0.12)	29.98 (0.34)	1.75 (0.31)	29.71 (0.39)	1.70	30.34 (0.29)
SiO_2	49.48 (0.20)	50.83 (0.42)	59.26 (0.32)	59.01 (0.24)	44.81 (0.30)	1.74 (0.20)	43.44 (0.46)	1.82	44.83 (0.36)
Cr_2O_3	17.74 (0.21)	14.99 (0.44)	0.00	1.17 (0.11)	25.54 (0.40)	95.89 (50)	25.02 (0.15)	96.03	24.22 (0.38)
Total	100.74	100.18	99.12	99.80	100.33	99.37	98.17	99.55	99.39
Formula units per given O									
O	12	12	3	12	12	3	12	3	12
Mg	3.526	3.600	1.001	3.969	3.257	0.065	3.303	0.063	3.316
Si	3.494	3.575	0.999	3.969	3.268	0.044	3.242	0.045	3.289
Cr	0.990	0.833	0.000	0.062	1.472	1.898	1.476	1.897	1.404
Total	8.011	8.008	2.001	8.000	7.997	2.007	8.021	2.006	8.009

P, GPa	16			17		18			
Run no.	2,398–50	2,418–15	2,399–10	2,408–100		2,415–100		2,438–60	2,415–10
Phase	Grt	Grt	Grt[a]	Grt	Esk	Grt	Ct	Grt[a]	Ak[a]
Number of points	4	4	3	5	2	6	3	5	4
MgO	32.47 (0.31)	38.16 (0.10)	38.95 (0.09)	30.50 (0.13)	3.02 (0.31)	31.19 (0.49)	24.46 (0.45)	31.97 (0.44)	38.51 (0.42)
SiO_2	48.67 (0.19)	57.22 (0.20)	57.61 (0.08)	45.69 (0.38)	3.84 (0.21)	46.45 (0.34)	3.52 (0.35)	47.32 (0.31)	57.39 (0.35)
Cr_2O_3	18.02 (0.17)	5.63 (0.39)	3.74 (0.05)	23.57 (0.30)	92.23 (0.56)	21.85 (0.30)	71.82 (0.53)	21.31 (0.23)	3.42 (0.40)
Total	99.16	101.04	100.30	99.56	99.09	99.49	99.80	100.60	99.32
Formula units per given O									
O	12	12	12	12	3	12	4	12	3
Mg	3.474	3.833	3.919	3.309	0.111	3.374	1.133	3.411	0.977
Si	3.496	3.858	3.891	3.328	0.095	3.373	0.110	3.390	0.977
Cr	1.023	0.300	0.200	1.357	1.799	1.254	1.765	1.206	0.046
Total	7.993	7.992	8.009	7.994	2.005	8.000	3.008	8.007	2.000

Table 2 continued

P, GPa	18		19						20
Run no.	2,410–30		2,530–100	2,531–30		2,531–15		2,530–5	2,406–70
Phase	Grt	Ak[a]	Grt	Grt	Ak	Grt	Ak	Ak[a]	Grt
Number of points	5	3	4	5	5	3	4	3	5
MgO	33.63 (0.36)	37.94 (0.30)	32.35 (0.12)	32.98 (0.21)	39.04 (0.25)	33.38 (0.16)	38.84 (0.34)	39.12 (0.48)	33.53 (0.28)
SiO_2	49.74 (0.28)	56.55 (0.35)	47.93 (0.24)	48.40 (0.19)	57.67 (0.31)	49.74 (0.30)	57.72 (0.14)	58.31 (0.26)	50.04 (0.21)
Cr_2O_3	17.09 (0.37)	5.71 (0.23)	19.99 (0.11)	17.69 (0.15)	3.59 (0.11)	17.73 (0.25)	3.63 (0.03)	2.24 (0.17)	17.39 (0.20)
Total	100.46	100.20	100.27	99.07	100.3	100.85	100.19	99.67	100.96
Formula units per given O									
O	12	3	12	12	3	12	3	3	12
Mg	3.540	0.961	3.447	3.532	0.981	3.505	0.977	0.985	3.512
Si	3.514	0.962	3.429	3.480	0.973	3.507	0.975	0.985	3.519
Cr	0.954	0.077	1.130	1.005	0.048	0.988	0.048	0.030	0.966
Total	2.000	8.006	8.008	8.017	2.003	8.000	2.001	2.000	7.998

P, GPa	20								
Run no.	2,402–100		2,407–90		2,402–50			2,407–30	
Phase	Grt	Ct	Grt	Ct	Grt	Brd	Ct	Grt	Brd
Number of points	5	1	4	2	5	4	2	4	3
MgO	32.81 (0.30)	24.53	33.23 (0.48)	24.42 (0.28)	32.85 (0.38)	36.64 (0.32)	23.97 (0.74)	33.12 (0.13)	37.16 (0.50)
SiO_2	48.68 (0.35)	3.68	49.41 (0.31)	3.81 (0.21)	48.51 (0.35)	54.24 (0.49)	3.88 (0.21)	49.32 (0.26)	55.24 (0.40)
Cr_2O_3	17.54 (0.29)	70.95	17.98 (0.49)	70.79 (0.35)	18.19 (0.23)	8.23 (0.13)	70.61 (0.76)	17.64 (0.24)	6.86 (0.73)
Total	99.03	99.15	100.62	99.02	99.55	99.11	98.45	100.08	99.26
Formula units per given O									
O	12	4	12	4	12	3	4	12	3
Mg	3.511	1.142	3.502	1.138	3.505	0.947	1.123	3.505	0.955
Si	3.497	0.115	3.495	0.119	3.475	0.942	0.122	3.505	0.953
Cr	0.996	1.752	1.005	1.749	1.030	0.113	1.755	0.991	0.093
Total	8.005	3.009	8.002	3.006	8.010	2.002	3.000	8.000	2.001

P, GPa	20	21				23		24	
Run no.	2,434–15	2,528–100		2,528–30	2,529–10	2,413–70		2,424–50	2,424–10
Phase	Brd	Brd	Ct	Brd	Brd	Brd[a]	Ct[a]	Brd	Brd
Number of points	5	3	1	4	5	3	3	3	2
MgO	37.93 (0.41)	36.66 (0.18)	21.39	37.09 (0.51)	39.14 (0.45)	35.66 (0.24)	20.73 (0.25)	36.05 (0.39)	39.07 (0.19)
SiO_2	56.39 (0.43)	54.24 (0.28)	0.00	54.94 (0.40)	57.66 (0.35)	53.17 (0.48)	0.00	53.96 (0.44)	57.36 (0.21)
Cr_2O_3	5.62 (0.54)	8.31 (0.21)	79.32	8.05 (0.31)	3.78 (0.32)	10.35 (0.44)	78.58 (0.35)	10.92 (0.67)	4.03 (0.18)
Total	99.94	99.21	100.71	100.08	100.58	99.18	99.31	100.93	100.46
Formula units per given O									
O	3	3	4	3	3	3	4	3	3.00
Mg	0.963	0.947	1.012	0.949	0.982	0.929	0.996	0.923	0.983
Si	0.962	0.941	0.000	0.944	0.971	0.929	0	0.927	0.968
Cr	0.076	0.114	1.992	0.109	0.050	0.143	2.003	0.148	0.054
Total	2.001	2.002	3.004	2.002	2.004	2.000	2.999	1.999	2.005

[a] Crystals studied by X-ray diffraction

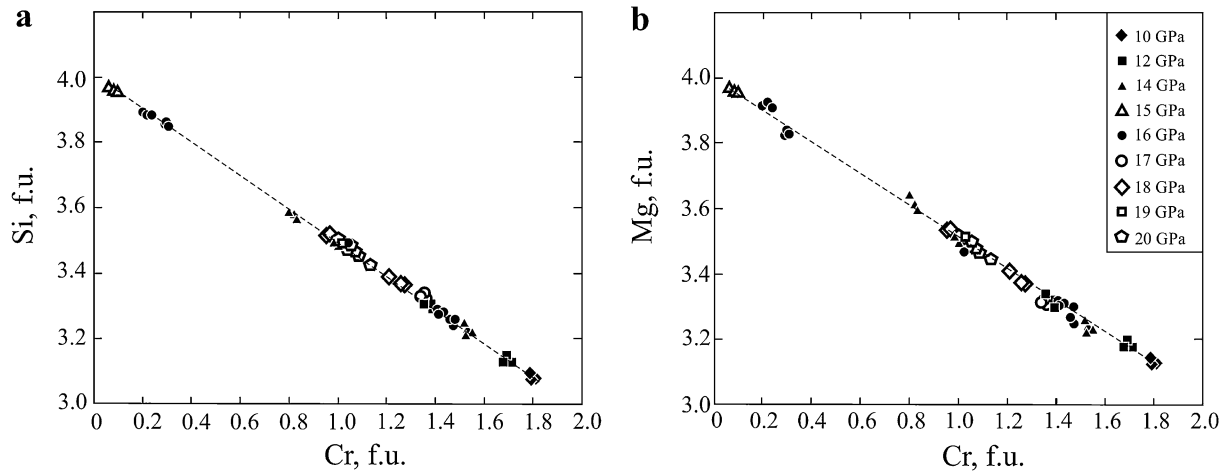

Fig. 6 Variations of Si, Mg, and Cr concentrations in garnets synthesized in the system $Mg_4Si_4O_{12}$–$Mg_3Cr_2Si_3O_{12}$ at 10–20 GPa and 1,600 °C

phase relations in the Maj–Knr system (Table 1; Fig. 4) and the composition of garnet (Table 2). It must be emphasized that pure knorringite was not synthesized over a wide pressure range (10–20 GPa). Garnet with the maximum chromium concentration (30.8 wt% Cr_2O_3), corresponding to ~90 mol% Knr, was obtained at 10 GPa. With increasing pressure, a decrease of the Cr concentration in garnet (18.19 wt% Cr_2O_3, ~50 mol% Knr at 20 GPa) is observed. As the maximum Cr content in garnet is clearly limited and consistent with earlier studies (Juhin et al. 2010; Zou and Irifune 2012), we conclude that it is not possible to synthesize pure knorringite. However, Klemme (2004) reported the absence of a majorite component (within the uncertainties of microprobe analysis) at the same parameters ($P = 16$ GPa, $T = 1{,}600$ °C). In our opinion, such differences may be likely dependent on synthesis conditions, because garnets nucleate sluggishly at high pressure.

The composition of $MgSiO_3$ *akimotoite* also depends on the starting composition and pressure (Table 2). An increase in the concentration of chromium in the starting material results in increase of the chromium content in akimotoite in the absence of other phases. The modal proportion and the Cr content of akimotoite associated with garnet increase with pressure. The maximal solubility of chromium (~5.7 wt% Cr_2O_3, 0.077 Cr pfu) in akimotoite was registered at 18 GPa. Cr shows negative correlations with both Mg and Si, consistent with a coupled Tschermak style substitution ($Mg^{2+} + Si^{4+} = 2Cr^{3+}$).

$MgSiO_3$ *bridgmanite* is characterized by higher chromium solubility (4–11 wt% Cr_2O_3, <0.148 Cr pfu) in comparison with akimotoite. Bridgmanite associated with Cr-rich garnet contains ≤5 wt% Cr_2O_3, whereas disappearance of garnet at $P > 21$ GPa results in a significant increase of the Cr concentration in bridgmanite (Table 2).

$MgCr_2O_4$ with a *calcium titanate-type structure* (Ct) associated with garnet and stishovite, synthesized in the pressure range from 18 to 20 GPa (Bindi et al. 2014c), is characterized by a small silicon admixture (up to 4 wt% SiO_2, 0.122 Si pfu). The concentration of Si in Ct increases with pressure. However, Ct in association with Brd at a pressure of >21 GPa does not contain Si.

Eskolaite in the $Mg_4Si_4O_{12}$–$Mg_3Cr_2Si_3O_{12}$ system was registered in association with garnet in the pressure range from 10 to 17 GPa for the knorringite-rich starting compositions. Esk is characterized by small admixtures of Mg and Si increasing with pressure (up to 3 wt% MgO, 0.111 Mg pfu and up to 3.8 wt% SiO_2, 0.095 Si pfu).

The influence of Cr on cell parameters of mantle phases and phase transitions

Five relatively large (up to 100 μm) garnet crystals of fair diffraction quality were selected for the X-ray single-crystal studies. The studied garnets belong to a wide compositional range from 3 to 90 mol% Knr (Table 3). All of them are characterized by cubic symmetry and space group $Ia\bar{3}d$.

The decrease in the concentrations of MgO and SiO_2 and increase of Cr_2O_3 in garnets provide evidence for the formation of almost complete series of solid solutions in the system of majoritic knorringite ($Mg_4Si_4O_{12}$–$Mg_3Cr_2Si_3O_{12}$), similarly to the majorite–pyrope system (Akaogi and Akimoto 1977). Figure 7 shows variations of the cubic lattice parameter in the majorite–knorringite system depending on the garnet composition. In contrast to the majorite–pyrope system, which shows a decrease in the cell parameter with increasing pyrope content, the majorite–knorringite join exhibits an increase in the cell parameter with increasing knorringite content, due to the average effect of the coupled substitution of $2Cr^{3+}$ (ionic radius

Table 3 Lattice parameters of garnets on the join majorite–knorringite

Run number	Garnet composition	Lattice parameters (Å)	V (Å^3)	References
Knorringite	$Mg_3Cr_2Si_3O_{12}$	11.6040	1,562.51	Ottonello et al. (1996)
2,526–100	$Mg_{3.10}Cr_{1.80}Si_{3.10}O_{12}$	11.5879 (2)	1,556.02 (3)	This study
H3420	$Mg_{3.21}Cr_{1.58}Si_{3.21}O_{12}$	11.5718 (1)	1,549.54 (2)	Bykova et al. (2014)
2,438–60	$Mg_{3.38}Cr_{1.24}Si_{3.38}O_{12}$	11.5445 (5)	1,538.61 (6)	This study
2,423–15	$Mg_{3.58}Cr_{0.84}Si_{3.58}O_{12}$	11.5187 (6)	1,528.33 (1)	This study
2,399–10	$Mg_{3.88}Cr_{0.24}Si_{3.88}O_{12}$	11.4725 (4)	1,510.00 (1)	This study
2,425–5	$Mg_{3.97}Cr_{0.06}Si_{3.97}O_{12}$	11.457 (3)	1,503.99 (5)	This study
Majorite	$Mg_4Si_4O_{12}$	11.5186 (4) (a); 11.4204 (4) (c)	1,515.25	Heinemann et al. (1997)

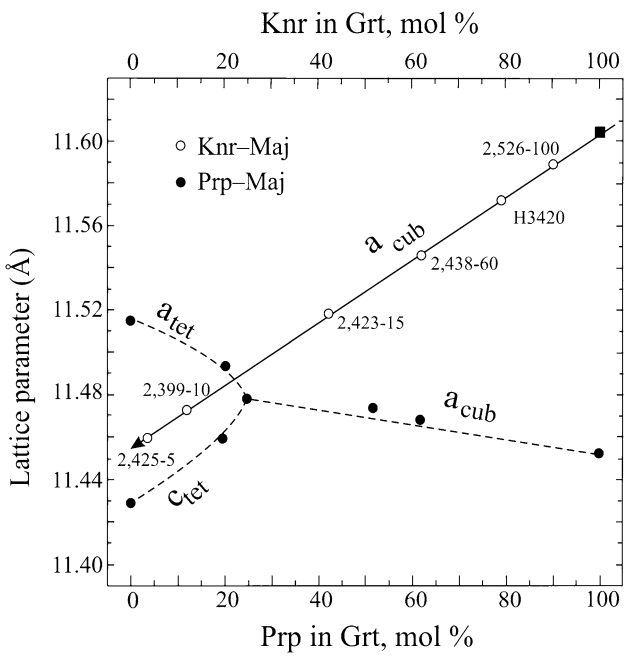

Fig. 7 Variations of unit cell parameters as a function of composition for a series of phases along the majorite ($Mg_4Si_4O_{12}$)–knorringite ($Mg_3Cr_2Si_3O_{12}$) join. The calculated cell parameter (*solid square*) of pure knorringite (Ottonello et al. 1996) and variations of unit cell parameters for the pyrope–majorite series (Parise et al. 1996) are shown for comparison. Sample H3420 is the synthetic garnet studied by Bykova et al. (2014)

r = 0.615 Å for the octahedral site) by Mg^{2+} (r = 0.72 Å) and Si^{4+} (r = 0.40 Å). The cell parameter for pure knorringite calculated by Ottonello et al. (1996) excellently matches our trend, plotting at the end of our line.

As it is evident from Fig. 7, the cubic/tetragonal transition at high majorite content (~75–80 mol% Maj) (Parise et al. 1996) along the majorite–pyrope join is not observed in the majorite–knorringite system, even at very high (97 mol%) majorite content. The shape of the high-θ reflections (800) collected at 2θ ≈ 28.6° for garnets from Samples 2,425–5 with 3 mol% Knr and 2,526–100 with 90 mol% of knorringite component (Fig. 8) shows that there is no split of the reflection induced by a twinning or tetragonal distortion. Our results are contrastingly different from the data on the majorite–pyrope system obtained by Heinemann et al. (1997), who reported splitting of the reflection (400) and explained this by ordering between Mg and Si in the octahedral sites, which is typical of tetragonal symmetry.

Our data show that even a small concentration of chromium stabilizes the cubic symmetry of garnet. On the other hand, Mg/Si disordering and the absence of merohedral twinning may be explained by kinetic conditions of garnet growth in experiment. Therefore, further structural studies are necessary to clarify the influence of Cr content on the majorite transition.

Based on our recent X-ray single-crystal diffraction studies of Cr-bearing akimotoite (Bindi et al. 2014a) and bridgmanite (Bindi et al. 2014a), *P–X* phase diagram of the system $Mg_4Si_4O_{12}$–$Mg_3Cr_2Si_3O_{12}$, and comparison with Al-bearing phases, we may consider the influence of Cr on the $MgSiO_3$ akimotoite/bridgmanite phase transition. The incorporation of chromium in $MgSiO_3$ akimotoite results in a general expansion of the unit cell, which is mostly controlled by the increase in the *a* cell parameter, whereas *c* is almost unaffected (Bindi et al. 2014a). The opposite tendency is observed for Al-bearing akimotoite (Fig. 9). An increase of the Al_2O_3 concentration in akimotoite results in a strong decrease in *c* and in a slight change of the *a* cell parameter, which is accompanied by a general decrease in the cell volume of Al-bearing akimotoite.

The cell parameters of $MgSiO_3$ bridgmanite change significantly with chromium incorporation in the mineral structure (Bindi et al. 2014b), whereas the influence of aluminum is not so strong (Fig. 9). Incorporation of both chromium and aluminum in bridgmanite results in an increase in the cell volume in comparison with that of pure $MgSiO_3$ bridgmanite (Dobson and Jacobsen 2004). An increase in the concentration of chromium is accompanied by a strong increase in the *a* parameter and a slight increase in the *b* and *c* parameters, whereas Al-bearing bridgmanite shows the opposite tendency: *b* and *c* increase and *a* slightly

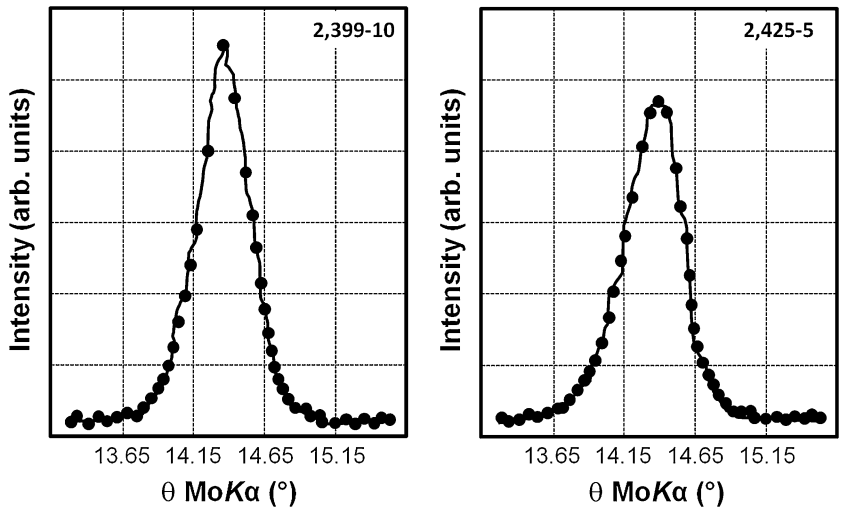

Fig. 8 Reflection (800) of the cubic structure of majoritic garnets collected at about $2\theta = 28.6°$ (Samples 2,399–10 and 2,425–5)

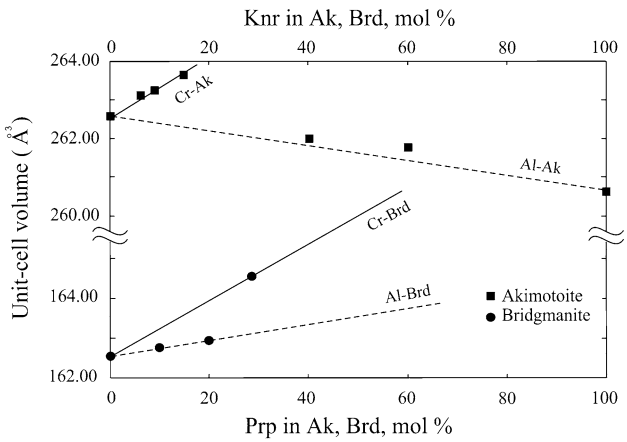

Fig. 9 Influence of chromium and aluminum on cell volumes of akimotoite (Kojitani et al. 2007) and bridgmanite (Dobson and Jacobsen 2004)

decreases (Kojitani et al. 2007). The discussed crystal-chemical data provide evidence for the significant influence of Cr on the $MgSiO_3$ akimotoite/bridgmanite phase transition. According to the results of our study, the stability field of Cr-bearing bridgmanite expands to the lower pressures (20 GPa) than that of Al-bearing and pure $MgSiO_3$ bridgmanite (21–22 GPa).

Implication for the mantle phase assemblages

The system $Mg_4Si_4O_{12}$–$Mg_3Cr_2Si_3O_{12}$ is of particular relevance to Cr incorporation in majoritic garnet and other mantle phases. Information on high chromium concentrations in mantle minerals may be obtained from the analysis of the data on inclusions in diamond and mantle peridotite xenoliths.

The combination of high Cr_2O_3, low CaO, and high Mg/(Mg + Fe) is typical of the most abundant class of garnets occurring as inclusions in natural diamonds. These garnets belong to the ultrabasic assemblage and correspond to dunitic and harzburgitic rock types. The concentration of chromium in garnet is traditionally used for estimation of pressure conditions favorable for the formation of diamonds (Grüter et al. 2006). As it is evident from the results of experimental studies summarized in (Bulatov et al. 1991; Stachel et al. 1998; Grütter 2001), the high Cr_2O_3 concentration observed in many peridotitic garnets requires a protolith with high Cr/Al. Such protolith may be formed as a residue of partial melting in the spinel peridotite stability field (Kesson and Ringwood 1989; Canil and Wei 1992; Stachel et al. 1998), and Cr-rich garnets would grow from such compositions upon subduction into the garnet stability field.

The presence of high Cr majoritic garnet inclusions in diamonds (e.g., Pokhilenko et al. 2004) is related to diamondiferous depleted ultrabasic rocks of the lithospheric mantle, and such diamonds were formed at depths exceeding 300 km. As the proportion of the majoritic component in knorringite significantly decreases with decreasing pressure, this could be an indicator of the pressures, where peridotitic inclusions were formed.

The $MgSiO_3$–$Mg_3Cr_2Si_3O_{12}$ join is relevant to the incorporation of a majorite component into knorringite garnet, since it proceeds according to the substitution $2Cr^{2+} = Mg + Si$ in the lowermost upper mantle and transition zone. The results of this study allow us to specify the stability range of Cr-bearing majoritic garnet. Although knorringite-bearing garnets are formed at pressure as low as 3 GPa (Malinovskii et al. 1975), they are mostly pyropic: Crystallization of knorringite-rich garnets is possible only at much higher pressure of ~8 GPa (Zou and Irifune 2012). Knorringite-rich garnet is associated with Px, Esk, and Ct and always contains an admixture of the majoritic end member (Fig. 4). For our Cr-rich starting materials, even

garnets formed close the lower pressure limit (10 GPa) contain over 10 mol% $Mg_4Si_4O_{12}$; at the upper pressure limit (20 GPa), the majorite component rises to over 50 mol%.

Our results are also directly applicable to the phase associations of podiform chromitites in the Luobusa ophiolite (Southern Tibet) containing diamond and other former ultrahigh-pressure minerals (Robinson et al. 2004; Dobrzhinetskaya et al. 2009; Yamamoto et al. 2009; Arai 2013). Yang et al. (2007) reported precursor stishovite for blade-shaped coesite. Robinson et al. (2004) suggested ringwoodite as a precursor of altered Mg–Fe silicate with an octahedral shape. Yamanoto et al. (2009) suggested a UHP precursor with a calcium ferrite structure originally formed at a pressure of >12.5 Ga and then decomposed to low-pressure chromite containing silicate exsolutions. Recently, based on the study of HPHT phase transitions of $MgCr_2O_4$, Ishii et al. (2014) suggested a lower-pressure origin of these chromitites because of the absence of the assemblage $Mg_2Cr_2O_5 + Cr_2O_3$ ($Fe_2Cr_2O_5 + Cr_2O_3$) in them. Although the formation of UHP chromitites is debatable, most of their characteristics are apparently consistent with a deep recycling origin. If so, Luobusa podiform chromitites may provide evidence for the very chromium-rich bulk compositions in the deep mantle.

Thus, our experiments show that mantle phases have the ability to accommodate high bulk rock Cr contents. The concentration of Cr_2O_3 in bridgmanite included in UHP diamond (1.2 wt%) (Harte et al. 1999) is much lower than the maximum Cr_2O_3 content obtained in this study. Even the most Cr-rich garnets observed to date (20 wt% Cr_2O_3) (Stachel and Harris 1997) still fall distinctly below the maximum Cr solubility observed in our experiments (30 wt% Cr_2O_3).

Conclusion

We have performed the first experimental study of phase relations along the pseudo-binary join $Mg_4Si_4O_{12}$–$Mg_3Cr_2Si_3O_{12}$ at 10–24 GPa and 1,600 °C and presented a *P–X* phase diagram involving majoritic knorringite and other chromium-bearing phases of the upper mantle, transition zone, and lower mantle of the Earth. Our experiments simulate Cr-rich phase assemblages found as inclusions in diamond, mantle xenoliths, and UHP podiform chromitites. It is demonstrated that Cr incorporation in major mantle phases (garnet, akimotoite, and bridgmanite) results in a strong increase in their cell parameters. Although our experiments were performed in the simplified SiO_2–MgO–Cr_2O_3 system and other components, such as Al, Fe, Ca, and Na may influence on the phase equilibria, it is believed that Cr exerts the significant control on phase relations and the proposed trends should also hold for more complex compositions.

Acknowledgments The constructive reviews of Thomas Stachel and an anonymous referee were very helpful for improving the quality of the manuscript. We thank Elena V. Guseva for electron microprobe analyses. This study was supported by the Russian Foundation for Basic Research (project nos. 12-05-00426, 12-05-33044, and 15-05-08261 to E.A. Sirotkina and A.V. Bobrov) and by the Grant-in-Aid for scientific Research (S) (Project No. 25220712 to T. Irifune). E.A. Sirotkina thanks Geodynamics Research Center, Ehime University, Matsuyama, Japan, for support of her visits in 2013 and 2014.

References

Akaogi M, Akimoto A (1977) Pyroxene-garnet solid-solution equilibria in the system $Mg_4Si_4O_{12}$–$Mg_3Al_2Si_2O_{12}$ and $Fe_4Si_4O_{12}$–$Fe_3Al_2Si_3O_{12}$ at high pressures and temperatures. Phys Earth Planet Inter 111:90–106

Akaogi M, Akimoto A (1979) High pressure phase equilibria in a garnet lherzolite, with special reference to Mg^{2+}–Fe^{2+} partitioning among constituent minerals. Phys Earth Planet Inter 19:31–51

Arai S (2013) Conversion of low-pressure chromitites to ultrahigh-pressure chromitites by deep recycling: a good inference. Earth Planet Sci Lett 379:81–87

Bindi L, Sirotkina EA, Bobrov AV, Irifune T (2014a) Chromium solubility in $MgSiO_3$ ilmenite at high pressure. Phys Chem Miner 41:519–526

Bindi L, Sirotkina EA, Bobrov AV, Irifune T (2014b) Chromium solubility in perovskite at high pressure: the structure of $(Mg_{1-x}Cr_x)(Si_{1-x}Cr_x)O_3$ (with x = 0.07) synthesized at 23 GPa and 1,600°C. Am Mineral 99:866–869

Bindi L, Sirotkina EA, Bobrov AV, Irifune T (2014c) X-ray single-crystal structural characterization of $MgCr_2O_4$, a post-spinel phase synthesized at 23 GPa and 1,600°C. J Phys Chem Solids 75:638–641

Bulatov V, Brey GP, Foley SF (1991) Origin of low-Ca, high-Cr garnets by recrystallization of low-pressure harzburgites. 5th International kimberlite conference, extended abstracts, CPRM, special publication 2/91:29–31

Bykova EA, Bobrov AV, Sirotkina EA, Bindi L, Ovsyannikov SV, Dubrovinsky LS, Litvin YuA (2014) X-ray single-crystal and Raman study of knorringite, $Mg_3(Cr_{1.58}Mg_{0.21}Si_{0.21})Si_3O_{12}$, synthesized at 16 GPa and 1,600°C. Phys Chem Miner 41:267–272

Canil D, Wei KJ (1992) Constraints on the origin of mantle-derived low Ca garnets. Contrib Mineral Petrol 109:421–430

Dobrzhinetskaya L, Wirth R, Yang J-S, Hutcheon I, Weber P, Green HW (2009) High pressure highly reduced nitrides and oxides from chromite of a Tibetian ophiolite. Proc Natl Acad Sci USA 106:19233–19238

Dobson DP, Jacobsen SD (2004) The flux growth of magnesium silicate perovskite single crystals. Am Mineral 89:807–811

Grüter H, Latti D, Menzies A (2006) Cr-saturation arrays in concentrate garnet compositions from kimberlite and their use in mantle barometry. J Petrol 47:801–820

Grütter HS (2001) The genesis of high Cr/Al garnet peridotite, with implications for cratonic crust: mantle architecture. The Slave-Kaapvaal workshop, Merrickville

Harte B, Harris JW, Hutchison MT, Watt GR, Wilding MC (1999) Lower mantle mineral associations in diamonds from Sao Luiz, Brazil. Mantle petrology: field observations and high pressure experimentation: a tribute to Francis R. (Joe) Boyd (The Geochemical Society, Houston) 6:125–153

Heinemann S, Sharp TG, Seifert F, Rubie DC (1997) The cubic-tetragonal phase transition in the system majorite ($Mg_4Si_4O_{12}$)–pyrope ($Mg_3Al_2Si_3O_{12}$), and garnet symmetry in the Earth's transition zone. Phys Chem Miner 24:206–221

Ionov DA, Doucet LS, Ashchepkov IV (2010) Composition of the lithospheric mantle in the Siberian Craton: new constraints from fresh peridotites in the Udachnaya-East kimberlite. J Petrol 51:2177–2210

Irifune T (1987) An experimental investigation of the pyroxene–garnet transformation in a pyrolite composition and its bearing on the constitution of the mantle. Phys Earth Planet Inter 45:324–336

Irifune T, Ohtani E, Kumazawa M (1982) Stability field of knorringite $Mg_3Cr_2Si_3O_{12}$ at high pressure and its implication to the occurrence of Cr-rich pyrope in the upper mantle. Phys Earth Planet Inter 27:263–272

Irifune T, Fujino K, Ohtani E (1991) A new high- pressure form of $MgAl_2O_4$. Nature 349:409–411

Irifune T, Kurio A, Sakamoto S, Inoue T, Sumiya H, Funakoshi K (2004) Formation of pure polycrystalline diamond by direct conversion of graphite at high pressure and high temperature. Phys Earth Planet Inter 143:593–600

Ishii T, Kojitani H, Fujino K, Yusa H, Mori D, Inaguma Y, Matsushita Y, Yamaura K, Akaogi M (2014) High-pressure high-temperature transitions in $MgCr_2O_4$ and crystal structures of new $Mg_2Cr_2O_5$ and post-spinel $MgCr_2O_4$ phases with implications for ultrahigh-pressure chromitites in ophiolites. Am Mineral. doi:10.2138/am-2015-4818

Juhin A, Morin G, Elkaim E, Frost DJ, Fialin M, Juillot F, Calas G (2010) Structure refinement of a synthetic knorringite, $Mg_3(Cr_{0,8}Mg_{0,1}Si_{0,1})_2(SiO_4)_3$. Am Mineral 95:59–63

Katsura T, Ito E (1989) The system Mg_2SiO_4–Fe_2SiO_4 at high pressure and temperatures: precise determination of stabilities of olivine, modified spinel and spinel. J Geophys Res 94:15663–15670

Kesson SE, Ringwood AE (1989) Slab-mantle interactions 2. The formation of diamonds. Chem Geol 78:97–118

Klemme S (2004) The influence of Cr on the garnet–spinel transition in the Earth's mantle: experiments in the system MgO–Cr_2O_3–SiO_2 and thermodynamic modeling. Lithos 77:639–646

Kojitani H, Katsura T, Akaogi M (2007) Aluminum substitution mechanisms in perovskite-type $MgSiO_3$: an investigation by rietveld analysis. Phys Chem Miner 34:257–267

Malinovskii IYu, Doroshev AM (1974) The system MgO–Al_2O_3–Cr_2O_3–SiO_2 at 1,200°C and 30 kbar. In: Godovikov AA, Sobolev VS (eds) Mineralogical experiments (1972–1973) [in Russian]. Inst Geol Geophys, Novosibirsk, pp 62–69

Malinovskii IYu, Doroshev AM, Ran EN (1975) The stability of chromium-bearing garnets pyrope: knorringite series. Experimental studies on the mineralogy (1974–1976). Institute of Geology and Geophysics of the Siberian Branch of AS USSR. Novosibirsk, pp 110–115

McKenna NM, Gurney JJ, Klump J, Davidson JM (2004) Aspects of diamond mineralisation and distribution at the Helam Mine, South Africa. Lithos 77:193–208

Meyer HOA (1987) Inclusions in diamond. In: Nixon PH (ed) Mantle xenoliths. Wiley, Chichester, pp 501–522

Nixon PH, Hornung G (1968) A new chromium garnet end member, knorringite from kimberlite. Am Mineral 53:1833–1840

Ono S, Yasuda A (1996) Compositional change of majoritic garnet in a MORB composition from 7 to 17 GPa and 1,400–1,600°C. Phys Earth Planet Inter 96:171–179

Ottonello G, Bokreta M, Sciuto PF (1996) Parameterization of energy and interactions in garnets: end-member properties. Am Mineral 81:429–447

Oxford Diffraction (2006) *CrysAlis* RED (Version 1.171.31.2) and ABSPACK in *CrysAlis* RED. Oxford diffraction Ltd, Abingdon, Oxfordshire, England

Parise J, Wang Y, Dwanmesia GD, Zhang J, Sinelnikov Y, Chmielowski J, Weidner DJ, Liebermann RC (1996) The symmetry of garnets on the pyrope ($Mg_3Al_2Si_3O_{12}$) – majoritc ($MgSiO_3$) join. Geophys Res Lett 23(25):3799–3802

Pokhilenko NP, Sobolev NV, Reutsky VN, Hall AE, Taylor LA (2004) Crystalline inclusions and C isotope rations in diamonds from the Snap Lake/King Lake kimberlite dyke system: evidence of ultradeep and enriched lithospheric mantle. Lithos 77:57–67

Pushcharovsky DYu, Pushcharovsky YuM (2012) The mineralogy and the origin of deep geospheres: a review. Earth Sci Rev 113:94–109

Ringwood AE (1966) The chemical composition and origin of the Earth. In: Hurley PM (ed) Advances in earth science. MIT Press, Cambridge, pp 287–356

Ringwood AE (1977) Synthesis of pyrope-knorringite solid-solution series. Earth Planet Sci Lett 36:443–448

Robinson PT, Bai W-J, Malpas J, Yang J-S, Zhou MF, Fang Q-S, Hu X-F, Cameron S, Staudigel H (2004) Ultrahigh-pressure minerals in the Luobusa ophiolite, Tibet, and their tectonic implications. In: Malpas J, Fletcher CJN, Ali JR, Aitchison JC (eds) Aspects of the tectonic evolution of China. J Geol Soc Special Publication vol 226, pp 247–271

Sobolev NV (1977) Deep-seated inclusions in kimberlites and the problem of upper mantle composition. In: Brown DA, Boyd FR (eds) English translation. American Geophysics Union, Washington, p 279

Sobolev NV, Logvinova AM, Zedgenizov DA, Seryotkin YV, Yefimova ES, Floss C, Taylor LA (2004) Mineral inclusions in microdiamonds and macrodiamonds from kimberlites of Yakutia: a comparative study. Lithos 77:225–242

Stachel T (2001) Diamonds from the asthenosphere and the transition zone. Eur J Mineral 13:883–892

Stachel T, Harris JW (1997) Diamond precipitation and mantle metasomatism-evidence from the trace element chemistry of silicate inclusions in diamonds from Akwatia, Ghana. Contrib Mineral Petrol 129:143–154

Stachel T, Viljoen KS, Brey G, Harris JW (1998) Metasomatic processes in lherzolitic and harzburgitic domains of diamondiferous lithospheric mantle: REE in garnets from xenoliths and inclusions in diamonds. Earth Planet Sci Lett 159:1–12

Taran MN, Langer K, Abs-Wurmbach I, Frost DJ, Platonov AN (2004) Local relaxation around $[6]Cr^{3+}$ in synthetic pyrope–knorringite garnets, $^{[8]}Mg_3^{[6]}(Al_{1-x}Cr_x^{3+})_2^{[4]}Si_3O_{12}$, from electronic absorption spectra. Phys Chem Miner 31:650–657

Taylor LA, Anand M (2004) Diamonds: time capsules from the Siberian Mantle. Chem Erde 64:1–74

Turkin AI, Sobolev NV (2009) Pyrope–knorringite garnets: overview of experimental data and natural parageneses. Russ Geol Geophys 50:1169–1182

Turkin AI, Doroshev AM, Malinovsky IY (1983) High-pressure and high-temperature investigation of the phases from garnet- bearing associations in the system MgO–Al_2O_3–Cr_2O_3–SiO_2. In: "Silicate systems under high pressures", Institute of Geology and Geophysics, Novosibirsk, 5–24 (in Russian)

Wijbrans CH, Niehaus O, Rohrbach A, Pöttgen R, Klemme S (2014) Thermodynamic and magnetic properties of knorringite garnet ($Mg_3Cr_2Si_3O_{12}$) based on low-temperature calorimetry and magnetic susceptibility measurements. Phys Chem Miner 41:341–376

Yamada A, Inoue T, Irifune T (2004) Melting of enstatite from 13 to 18 GPa under hydrous conditions. Phys Earth Planet Inter 147:45–56

Yamamoto S, Komiya T, Hirose K, Maruyama S (2009) Coesite and clinopyroxene exsolution lamellae in chromites: in situ ultrahigh-pressure evidence from podiform chromitites in the Luobusa ophiolite, southern Tibet. Lithos 109:314–322

Yang JS, Dobrzhinetskaya L, Bai WJ, Fang QS, Robinson PT, Zhang J, Green HW (2007) Diamond- and coesite-bearing chromitites from the Luobusa ophiolite, Tibet. Geology 35:875–878

Zou Y, Irifune T (2012) Phase relations in $Mg_3Cr_2Si_3O_{12}$ and formation of majoritic knorringite garnet at high pressure and high temperature. J Mineral Petrol Sci 107:197–205